Open Ceramics 22 (2025) 100764

Contents lists available at ScienceDirect

Open Ceramics

journal homepage: www.sciencedirect.com/journal/open-ceramics

Rapid synthesis of manganese tetraboride (MnB_4) using reactive spark plasma sintering

S.B. Dhuban [a,b], Hyoung-Won Son [a,*], Takao Mori [a,b,*]

[a] Research Center for Materials Nanoarchitectonics (MANA), National Institute for Materials Science (NIMS), Namiki 1-1, Tsukuba 305-0044, Japan
[b] Graduate School of Pure and Applied Sciences, University of Tsukuba, Tennodai 1-1-1, Tsukuba 305-8671, Japan

ARTICLE INFO

Keywords:
Reactive spark plasma sintering
SPS
Manganese
Boride

ABSTRACT

In this work, we report a rapid synthesis method for polycrystalline transition-metal tetraborides using reactive spark plasma sintering (R-SPS). This method was demonstrated on the synthesis of manganese tetraboride (MnB_4) in a short time, 30 min. Starting powders with variable B/Mn molar ratios (4.1, 4.5, 5.0, and 8.0) were subjected to 12 h of high-energy ball milling (HEBM), followed by synthesis and consolidation in a single step using R-SPS in a dynamic vacuum atmosphere. Phase purity was confirmed by powder X-ray diffraction (PXRD); MnB_4 was obtained for B/Mn molar ratio of 4.5 and higher in the temperature range of 850 – 1080 °C, while the lower B/Mn molar ratio (4.1) resulted in a mixed-phase (Mn_3B_4 + MnB_4) sample. The crystal structure and lattice parameters estimated from PXRD agree well to those reported for single-crystal MnB_4. Thermogravimetric differential thermal analysis (TG/DTA) revealed that MnB_4 is stable in air up to 400 °C.

1. Introduction

Due to its electron deficiency, atomic size, electronegativity, and ionization energy boron exhibits interesting chemistry, and boron compounds adopt covalent bonding motif ranging from 1D chains to 2D sheets to 3D networks [1–4]. Boron-based compounds exhibit a variety of useful properties, such as superconductivity [5], high bulk modulus, high hardness, high melting points, good thermal stability, excellent electrical and thermal transport properties, and thermoelectricity [6–14]. Despite their huge potential and extensive fundamental research, applications of boride-based compounds are still limited.

Metal borides have gained an increasing interest since the discovery of superhardness and superconductivity in some phases, i.e., ReB_2 [6] and MgB_2 [5]. Transition metal borides, in particular, are attractive because of their relative ease of synthesis in comparison to traditional covalently bonded materials such diamond and cubic boron nitride (c-BN) which can only be obtained under high-pressure high--temperature (HPHT) conditions [15]. Cost, complexity, and sample size limitations are the main disadvantages of the HPHT method. Transition metal tetraborides have been synthesized using both HPHT and arc melting method, i.e., WB_4 [7,16,17], FeB_4 [18], CrB_4 [19]. However, a complete melt and re-melt (3- 5 times) of the reactants are required in the case of arc melting method to achieve a homogenous sample. Therefore, arc melting is not a viable synthesis method for phases that undergo phase decomposition before melting, i.e., MnB_4.

Spark plasma sintering (SPS) is a rapid sintering method that uses the combination of relatively low uniaxial pressure and pulsed electric current (DC) to heat and sinter the powder inside a die. SPS offers some advantages such as shorter sintering time, high heating rates, grain growth suppression, lower sintering temperatures, and energy reduction [20]. Chemical reactions can also be performed inside the SPS die to synthesize and densify materials in a single step in the so-called reactive spark plasma sintering (R-SPS). Additionally, accurate temperature control makes R-SPS attractive for the synthesis of metastable compounds. R-SPS synthesis technique has been focused on transition metal diborides [21–30] and high-entropy diborides [31,32]. However, R-SPS synthesis of transition-metal tetraborides has not been reported in the literature.

MnB_4 crystallizes in a unique three-dimensional boron atom framework reminiscent of that of carbon atoms in diamond structure (Fig. 1). At room temperature, MnB_4 crystallizes in a monoclinic crystal structure which can be described as a distorted variant of the body-centered tetragonal carbon structure (bct-C_4) in which each boron atom is surrounded by four other boron atoms [33]. Early X-ray diffraction data obtained in the late 1960s by Andersson and Carlsson [34] indexed MnB_4 to space group C2/m, but later studies have shown that it belongs

* Corresponding authors.
E-mail addresses: SON.Hyoungwon@nims.go.jp (H.-W. Son), MORI.Takao@nims.go.jp (T. Mori).

https://doi.org/10.1016/j.oceram.2025.100764
Received 25 January 2025; Received in revised form 4 March 2025; Accepted 10 March 2025
Available online 10 March 2025

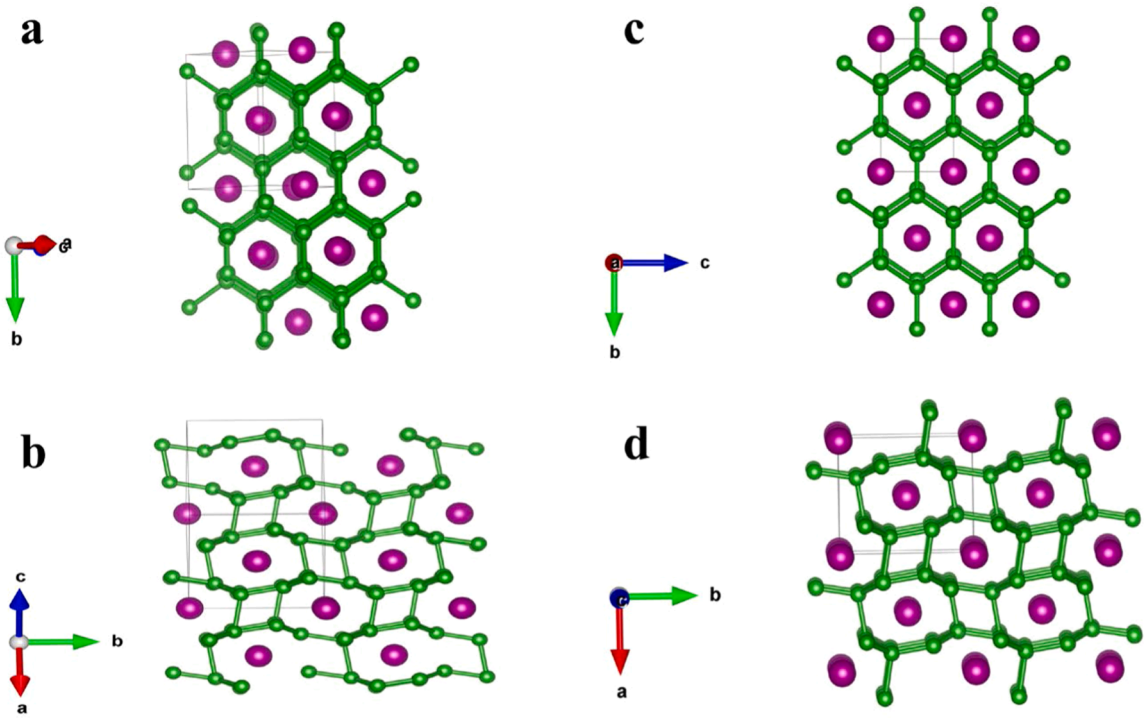

Fig. 1. Crystal structure of room-temperature monoclinic MnB_4 (a, b) and high-temperature orthorhombic MnB_4 (c, d). Mn atoms are shown in purple, B atoms in green.

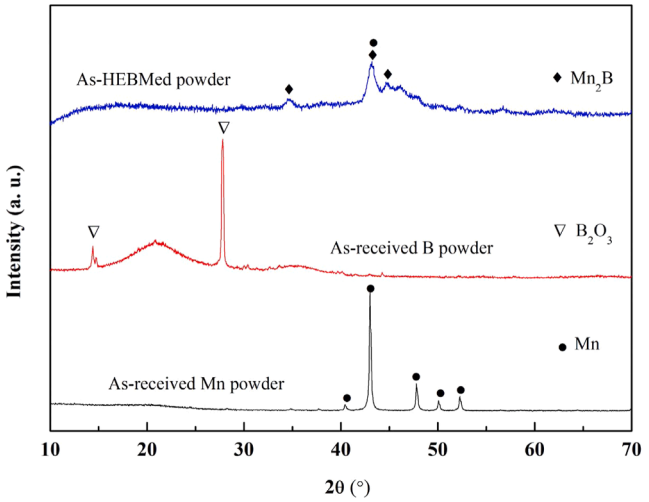

Fig. 2. PXRD patterns of the as-received Mn, as-received amorphous B, and as-HEBMed powder mixture. The HEBM was carried out for 12 h. During the HEBM, B partially reacted with Mn to form Mn_2B.

to space group $P2_1/c$, at room temperature [33,35,36]. High-temperature X-ray diffraction revealed that the room-temperature monoclinic MnB_4 undergoes a reversible phase transformation to an orthorhombic phase at around 377 °C [33]. Due to the unusual crystal structure, theoretical studies predicted that MnB_4 could be a superhard material [37,38], but experimental investigations on polycrystalline MnB_4 synthesized using HPHT method [35,36,39] have yielded the highest hardness of 37.4 GPa in the asymptotic region. Asymptotic hardness is defined as a hardness obtained at high loads which corresponds to the asymptotic leveling of the hardness-load curve [40]. Although MnB_4 is not superhard, it is still one of the hardest transition metal borides. The high hardness, low density (4.45 g/cm^3), manganese

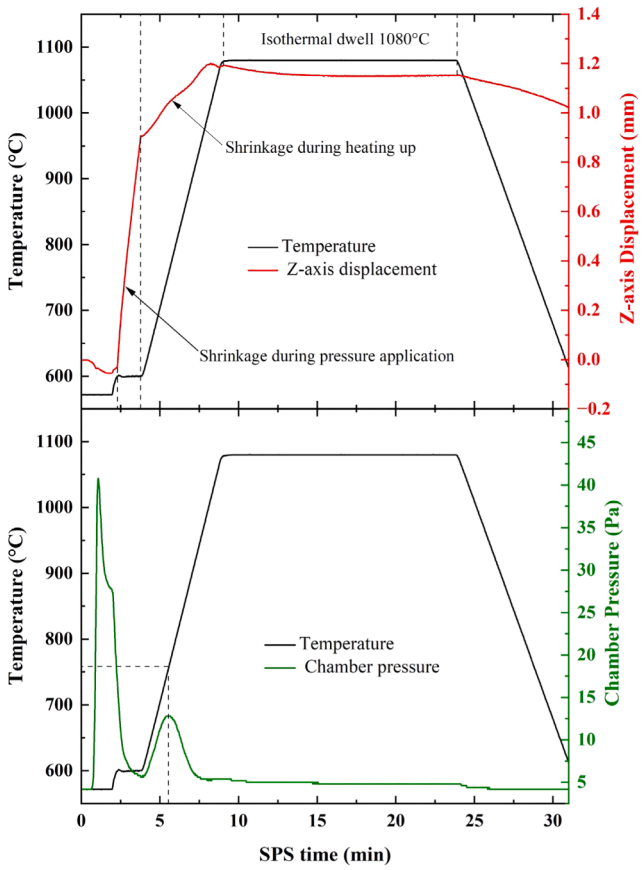

Fig. 3. SPS temperature, Z-axis displacement, and chamber pressure profiles during R-SPS of MnB_4 with molar ratio of 4.5 under dynamic vacuum condition. Heating rate of 100 °C/min and 80 MPa of uniaxial pressure were applied.

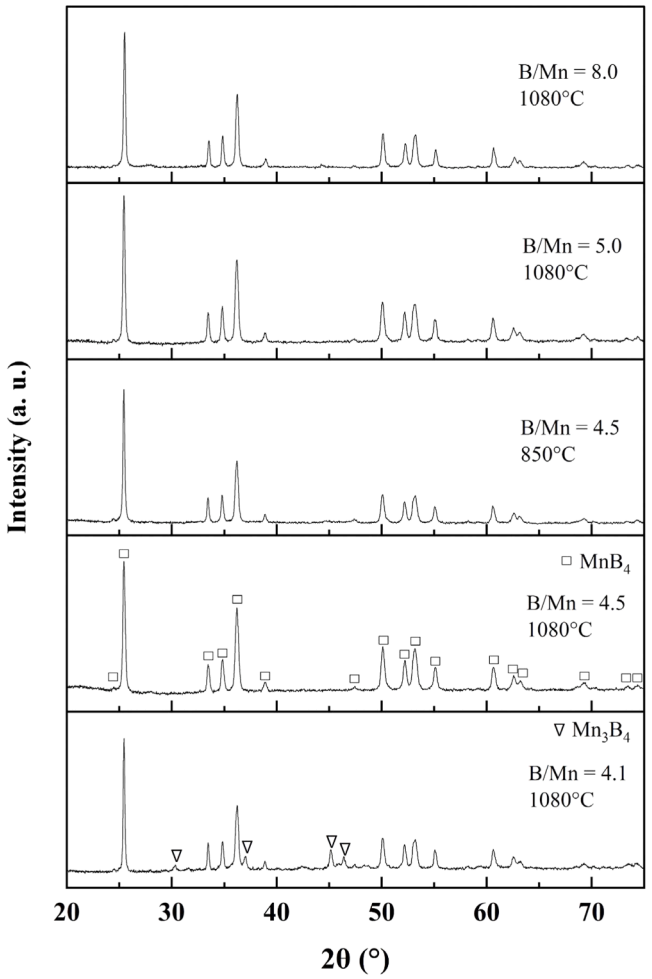

Fig. 4. PXRD patterns of MnB_4 synthesized via R-SPS with different B/Mn molar ratios: 4.1, 4.5, 5.0 and 8.0. The samples were subjected to R-SPS at either 850 °C or 1080 °C for 15 min with a heating rate of 100 °C/ min under 80 MPa of uniaxial pressure in a dynamic vacuum atmosphere. MnB_4 was obtained at a B/Mn molar ratio of 4.5 and above, in the temperature range of 850 °C −1080 °C.

abundance and relatively low-cost renders MnB_4 an interesting hard compound.

MnB_4 has only been synthesized using either HPHT method or a lengthy process using solid-state reaction in a silica ampoule with iodine as a mineralizer (14 days) [33]. Based on the Mn-B binary phase diagram, MnB_4 decomposes into $MnB_2 + B$ at around 1375 °C under atmospheric pressure [41], therefore accurate temperature control during the synthesis process is necessary to obtain MnB_4. In this study, we show that R-SPS is a viable cost-effective rapid synthesis method for polycrystalline MnB_4 with low amount of excess boron. Furthermore, this is the first report on the synthesis of a transition metal tetraboride using R-SPS, to the best of our knowledge.

2. Materials and methods

The starting materials used herein were amorphous boron (0.8 μm, 99 %, SB Boron Corp., USA) and crystalline manganese (75 μm, 99.95 %, Wako Co., Ltd., Japan) powders. The as-received starting materials were weighed and loaded into a jar under argon atmosphere in a glove box to avoid additional oxidation. Various B/Mn molar ratios with variable amounts of excess boron (B/Mn = 4.1, 4.5, 5.0 and 8.0) powder mixtures were subjected to high-energy ball milling (HEBM; 8000 M mixer/mill, SPEX SamplePrep, USA) to enhance the reactivity and densification by reducing the powder crystallite size. The HEBM process was carried out for 15 h with 1 h of running interval and 15 min of resting time.

MnB_4 pellets were synthesized in one step using R-SPS (Dr. Sinter 322 lx, Fuji Denpa Koki Co., Ltd., Japan); 0.5 g of each as-HEBM mixture was poured into a graphite die and was subjected to R-SPS at either 850 °C or 1080 °C for 15 min in a dynamic vacuum atmosphere (6 Pa chamber pressure), with 100 °C/min of heating rate under 80 MPa (6.3 kN) of uniaxial applied pressure. The temperature was measured using infrared pyrometer (CHINO, IR-AH, Japan) focused on a hole on the lateral side of the die, and the distance between the pyrometer spot and the sample was 5 mm. The sintered samples were ground on both sides with diamond abrasive papers (grit 400 and 1000) to remove graphite sheet. Apparent densities and open porosity percentages of the sintered samples were determined based on Archimedes' principle using boiling method according to JIS R 1634 standard. The sintered samples were crushed into sub 40 μm powder by an agate pestle and a mortar for powder X-ray diffraction (PXRD) for constituent phase and crystal structure analyses. The PXRD was performed via X-ray diffractometer (MiniFlex, Rigaku, Japan) using Cu-K_α radiation source ($\lambda = 1.5406$ Å) at 40 kV and 15 mA. The 2θ scanning range was set from 20° to 75° at 1°/min of a scan speed with 0.02° step. To determine the crystal structure parameters, profile matching refinement was performed on the collected PXRD using FullProf software. Microstructural observation on the fracture surface of the sintered samples was conducted using field emission scanning electron microscope (FE-SEM, SU8000, Hitachi, Japan). Thermal stability measurement was conducted in air using thermogravimetric differential thermal analysis (TG/DTA6200, Exstar6000, Hitachi, Japan). The powder sample (10 mg) was heated at a rate of 5 °C/min from room temperature to 700 °C. The temperature was held at 700 °C for 10 min after which the heating was turned off and it naturally cooled down to room temperature.

3. Results and discussions

The PXRD patterns of the as-received Mn, as-received amorphous B, and the as-HEBMed mixture are presented in Fig. 2. While the as-received Mn powder is pure, the as received amorphous B exhibits a pronounced crystalline B_2O_3 peaks because the surface of fine amorphous B particles can easily be oxidized when exposed to air. However, the as-HEBMed powder mixture consists of only Mn and Mn_2B which indicates a partial reaction between Mn and amorphous B occurred during the 12 h of HEBM process. The absence of B_2O_3 crystalline peaks after HEBM could be due to amorphization of B_2O_3 caused by HEBM. Studies have shown that HEBM can cause amorphization in pure elements and intermetallic compounds by mechanical deformation [42, 43].

One advantage of the R-SPS is the capability of recording important parameters, such as temperature profile; Z-axis displacement (shrinkage); and chamber pressure, which provide useful insight into the synthesis process. The R-SPS temperature, Z-axis displacement and chamber pressure profiles of MnB_4 are presented in Fig. 3, which was synthesized with B/Mn molar ratio of 4.5 in a dynamic vacuum atmosphere at 1080 °C with heating rate of 100 °C/min under 80 MPa of uniaxial pressure.

The starting temperature shown in Fig. 3 is 572 °C because the infrared pyrometer is only capable of measuring temperatures above 572 °C, and this temperature could be reached after around 2 min of starting the current application. Then the temperature was held at 600 °C for stabilization, and a pressure of 80 MPa was applied after which the temperature was increased to the synthesis temperature with a rate of 100 °C/min, and then held for 15 min of isothermal dwell time at the synthesis temperature. The linear temperature profile indicates that this reaction between B and Mn progressed as an externally controlled reaction (ESR) rather than a self-sustained reaction (SSR). In the ESR, the exothermic reaction heat is dissipated, and the sintering media temperature equals that of the furnace which is evident by the absence of

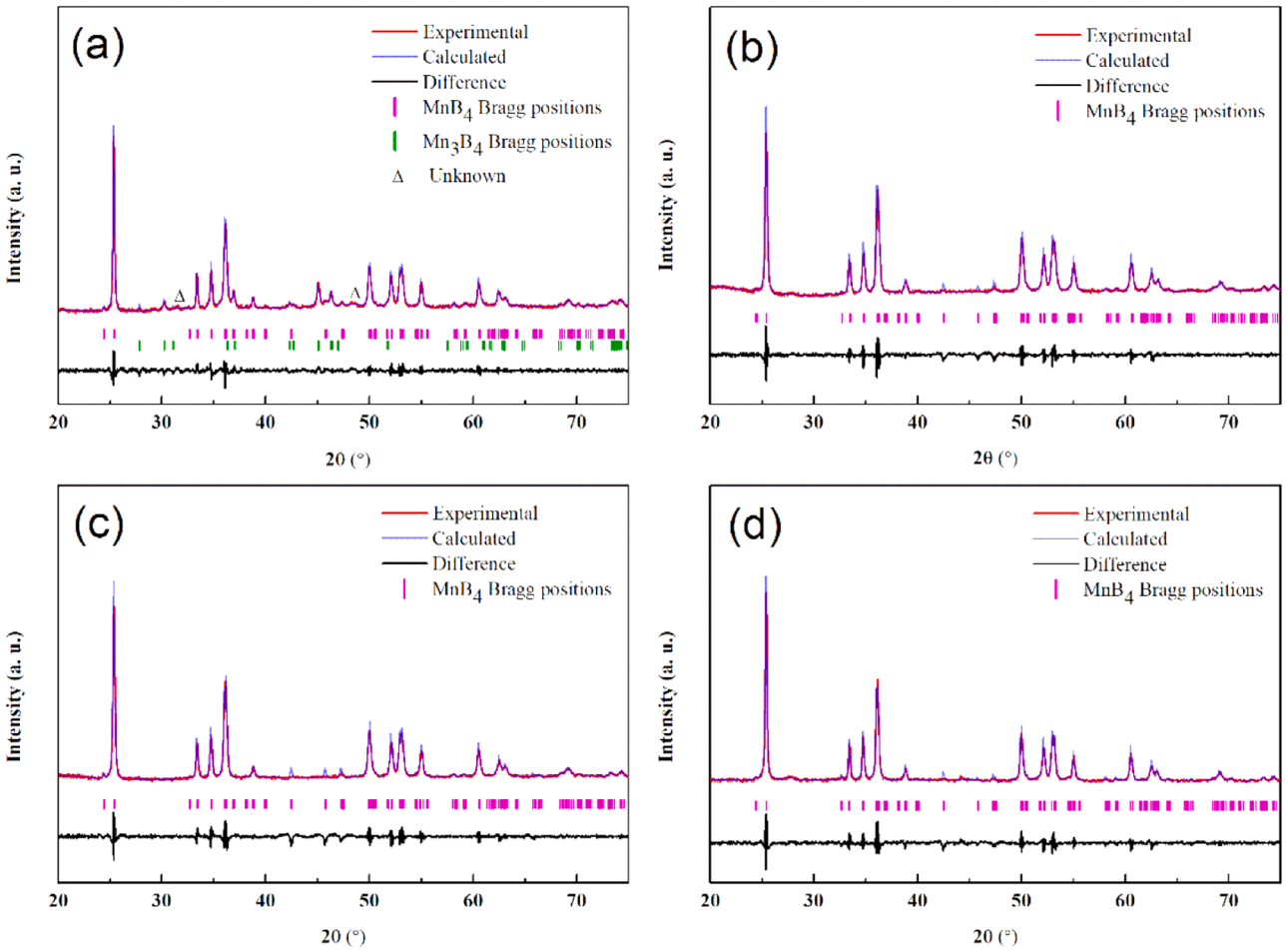

Fig. 5. Profile matching refinement on the PXRD patterns of MnB_4 synthesized with different B/Mn molar ratios: 4.1 (a), 4.5 (b), 5.0 (c) and 8.0 (d). The samples were synthesized using R-SPS at 1080 °C for 15 min with a heating rate of 100 °C/ min under 80 MPa of uniaxial pressure in a dynamic vacuum atmosphere.

Table 1
Effect of stoichiometry on the crystal structure parameters of MnB_4; the samples were synthesized using R-SPS at 1080 °C for 15 min with a heating rate of 100 °C/min under 80 MPa of uniaxial pressure in a dynamic vacuum atmosphere.

	Nominal molar ratio (B/Mn)			
	4.1	4.5	5.0	8.0
Crystal system	Monoclinic			
Space group	$P2_1/c$			
***a* (Å)**	5.485	5.474	5.480	5.479
***b* (Å)**	5.365	5.362	5.366	5.364
***c* (Å)**	5.504	5.500	5.505	5.503
β (°)	115.261	115.213	115.148	115.126
Lattice volume (Å^3)	146.486	146.052	146.534	146.426
Bragg R-factor	1.27	1.56	1.51	2.21

sudden temperature changes [44]. The MnB_4 formation reaction between Mn and B is a low heat-generating exothermic reaction with ΔH value of –27.89 kJ/mol [45].

The Z-axis displacement curve can be divided into three regions: displacement due to force application, heating up, and isothermal dwell region. The sample underwent a rapid shrinkage corresponding to the increase in the displacement due to the application of 80 MPa (6.3 kN) uniaxial pressure. Then the sample underwent moderate shrinkage during the temperature ramp up to the maximum temperature. At the isothermal dwell region, the displacement decreases with holding time because of the thermal expansion of graphite punches and spacers system by Joule heating. There is an increase in the chamber pressure to ≈

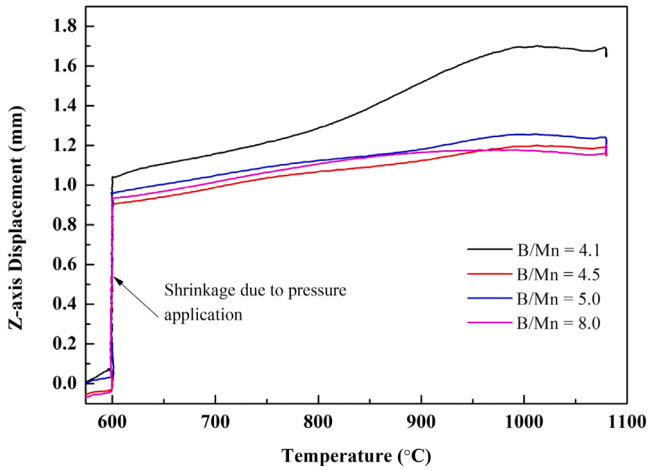

Fig. 6. Z-axis displacement profile as a function of stoichiometry. The samples were synthesized using R-SPS at 1080 °C for 15 min with a heating rate of 100 °C/ min under 80 MPa of uniaxial pressure in a dynamic vacuum atmosphere.

40 Pa after around 1 to 2 min of starting the sintering process which could be due to the evaporation of moisture contained within the powder sample and the die/punch/spacers assembly. Additionally, a low vapor pressure of B_2O_3 could be attributed to the evaporation of liquid B_2O_3 which melts at 450 °C. At ≈ 750 °C, there is a slight increase

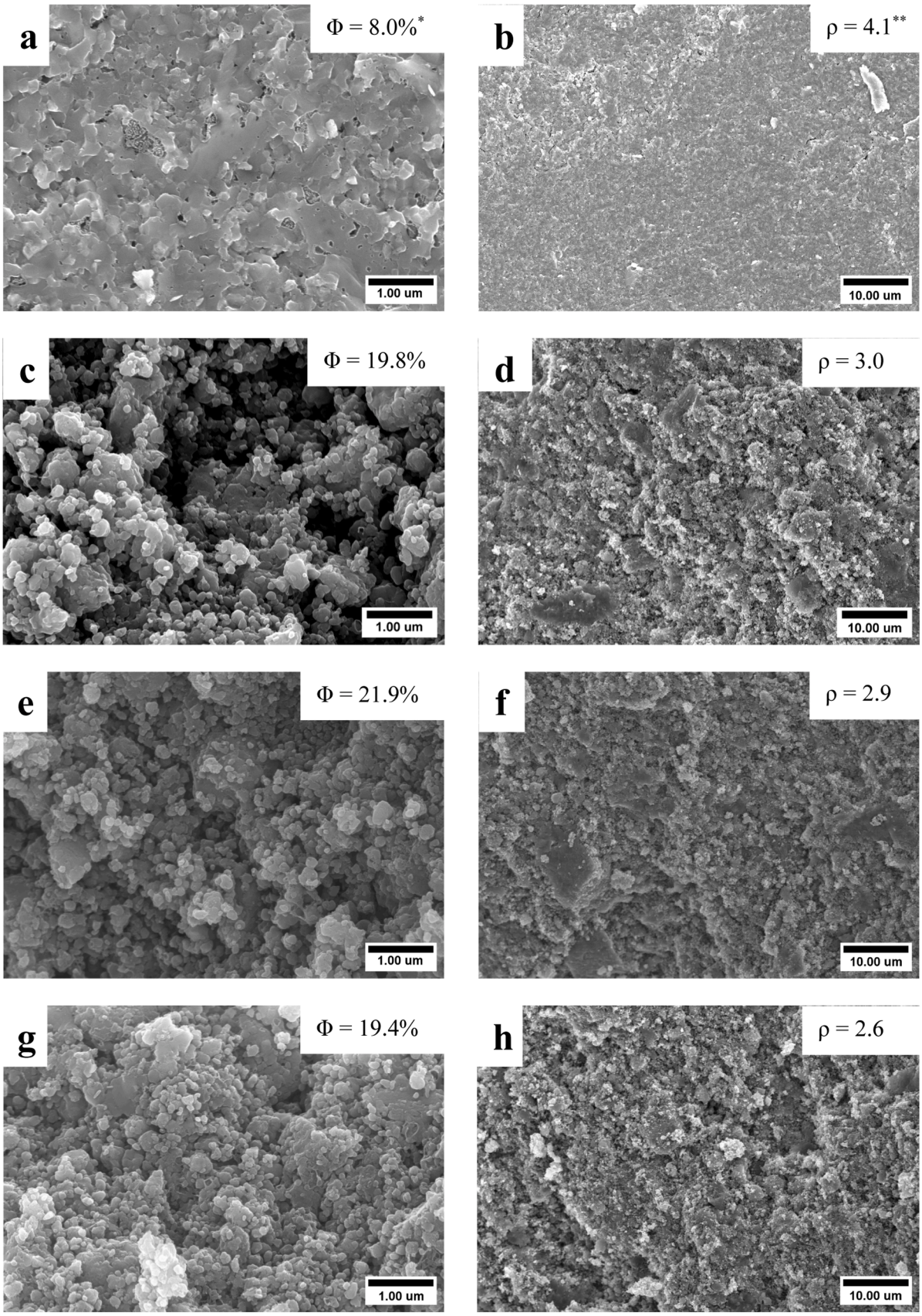

Fig. 7. SEM images of the fracture surface of MnB_4 synthesized with variable B/Mn molar ratios: 4.1 (a,b), 4.5 (c,d), 5.0 (e,f) and 8.0 (g,h). The samples were subjected to R-SPS at 1080 °C for 15 min in a dynamic vacuum atmosphere with a heating rate of 100 °C/min under 80 MPa of uniaxial pressure. The theoretical density of MnB_4 is 4.45 g/cm^3. * Φ represents open porosity (%). ** ρ represents apparent density (g/cm^3).

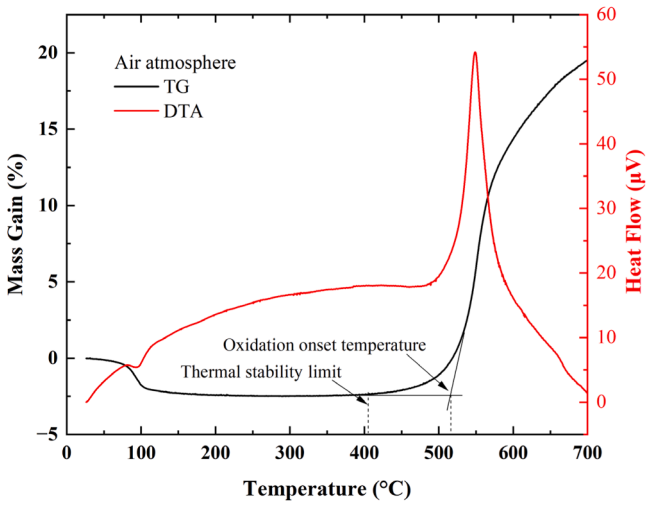

Fig. 8. Thermal stability in air obtained from thermogravimetric differential thermal analysis (TG/DTA) of MnB_4 sample synthesized with B/Mn molar ratio of 4.5 using R-SPS at 1080 °C for 15 min in a dynamic vacuum atmosphere. The graph shows that MnB_4 is stable in air up to ≈ 400 °C.

in the chamber pressure to ≈ 12 Pa which could be due to MnB_4 formation exothermic reaction accompanied by gas release [46].

Based on the Mn-B binary phase diagram [41], at a B/Mn molar ratio of 2.3 – 4.0, $MnB_4 + Mn_3B_4$ coexist below 1100 °C, and $MnB_4 + B$ are present above B/Mn value of 4.0 below 1375 °C under atmospheric pressure. In this experiment, various molar ratios (4.1, 4.5, 5.0 and 8.0) were used to synthesize MnB_4; mixed phase ($MnB_4 + Mn_3B_4$) sample was obtained at molar ratio of 4.1 at 1080 °C as indicated in Fig. 4, which presents the PXRD patterns of the samples synthesized with variable B/Mn molar ratios at different temperatures. The presence of the lower boride phase (Mn_3B_4) could be due to stoichiometry shift caused by the evaporation of B_2O_3 contained in the starting amorphous B powder under dynamic vacuum atmosphere. Therefore, excess boron is necessary to prevent the formation of the lower boride phase, Mn_3B_4.

Increasing the amount of excess boron to B/Mn molar ratio of 4.5, 5.0 and 8.0 produced MnB_4 in the temperature range of 850 °C - 1080 °C (Fig. 4). In addition to MnB_4, samples presumably contain various amounts of B which cannot be detected by the XRD. The PXRD patterns of as-HEBMed powder mixture in Fig. 2 show that B partially reacted with Mn to form Mn_2B after which the reactants transformed to MnB_4 during the R-SPS process, ~ 30 min. The PXRD data in Fig. 4 shows that MnB_4 could be synthesized at 850 °C up to 1080 °C. Profile matching refinement was performed on samples synthesized with variable B/Mn molar ratios, and the obtained lattice parameters are in a good agreement with those of single crystal MnB_4 (ICSD-426,691), space group $P2_1/c$, obtained at ambient temperature. Fig. 5 shows the refined PXRD patterns and Table 1 shows the lattice parameters of MnB_4 obtained via profile matching method. The lattice parameters presented in Table 1 show no significant variation with stoichiometry which imply that the excess B contained in the samples with B/Mn molar ratios of 4.5, 5.0 and 8.0 form a secondary phase.

The synthesis cycle of this R-SPS synthesis was completed in around 30 min including holding time (15 min) at the synthesis temperature and cooling down. In comparison, a solid-state reaction in a silica ampoule with iodine as a mineralizer was used to synthesize pure polycrystalline MnB_4 at 1000 °C and the synthesis time was 14 days [33]. Furthermore, using HTHP method, pure polycrystalline MnB_4 was also synthesized under 3 GPa of applied pressure and the synthesis time was in the range of 4 – 240 h [35]. HPHT experiments with short holding time (15 min) at 1527 °C were also carried out but MnB_4 was only obtained with excessive amount of excess B with B/Mn molar ratio of 12.0 [39]. Indeed, excess boron is often required in the synthesis of transition-metal tetraborides to prevent the formation of lower boride phases particularly in the case of arc melting synthesis. WB_4 was synthesized using the arc melting method with molar ratio (B/W) of 12.0 to prevent the formation of the thermodynamically favorable WB_2 [7,47]. Excess B results in the formation of amorphous/crystalline boron secondary phase which could alter the materials properties. Further optimization of the R-SPS reported in this study could eliminate the need for excess boron if pristine material is desired.

The Z-axis displacement as a function of stoichiometry is shown in Fig. 6. The samples with B/Mn molar ratios of 4.5, 5.0 and 8.0 showed similar displacement changes while the sample with B/Mn molar ratio of 4.1 showed significantly different displacement curve. The sample with B/Mn molar ratio of 4.1 experienced a maximum displacement of ≈ 1.6 mm while the samples with B/Mn molar ratios of 4.5, 5.0 and 8.0 experienced maximum displacements of ≈ 1.1 mm. Fig. 7 shows SEM images of fracture surface of the samples synthesized with variable molar ratios. All samples show equiaxed grains. The samples synthesized with B/Mn molar ratios of 4.5, 5.0 and 8.0 (Fig. 7c, d, e, f, g and h) exhibit similar microstructure with similar open porosity values of 19.8, 21.9, and 19.4 %, respectively. In comparison, the sample synthesized with B/Mn molar ratio of 4.1 (Fig. 7a and b) exhibits higher density with lower open porosity value of 8.0 %. The difference in the displacements and microstructures among the samples could be due to the presence of the easier-to-sinter Mn_3B_4 phase in the sample with B/Mn molar ratio of 4.1. Considering the results of the refinement, the sample with B/Mn molar ratio of 4.1 (Fig. 7a and b) is constituted by MnB_4 with Mn-rich phase, Mn_3B_4, while those with B/Mn molar ratios of 4.5, 5.0 and 8.0 (Fig. 7c, d, e, f, g and h) are constituted by MnB_4 with secondary B phase.

Previous study showed that MnB_4 exhibits high asymptotic hardness (37.4 GPa) [35] which makes it one of the hardest transition-metal borides. Thermal stability is an important property for hard materials used in machining applications as it indicates the long-term stability and performance of the material. Thermal stability in air of MnB_4 synthesized with B/Mn molar ratio of 4.5 was studied using TG/DTA and the results are plotted in Fig. 8. The mass loss and endothermic peak are observed at around 70 – 100 °C due to removal of moisture. At around 520 °C, there is a rapid weight gain accompanied by an exothermic peak which marks the onset oxidation temperature of MnB_4. The weight gain could be attributed to manganese oxide formation. MnB_4 is stable in air up to ≈ 400 °C which is similar to the both the traditional abrasive material tungsten carbide (WC) and tungsten tetraboride (WB_4) [47].

4. Conclusion

Manganese tetraboride (MnB_4) has been successfully synthesized rapidly using R-SPS in 30 min. PXRD patterns of the as-HEBMed mixtures showed that B partially reacted with Mn to form Mn_2B during the 12 h HEBM process. The R-SPS of the as-HEBMed mixtures was carried out in the temperature range of 850 °C - 1080 °C with isothermal dwell time of 15 min at the synthesis temperature. The sample with B/Mn molar ratio of 4.1 consists of mixed-phase ($Mn_3B_4 + MnB_4$) while the samples with B/Mn molar ratio of 4.5 and higher mainly consist of MnB_4 phase. It was also revealed that MnB_4 is stable in air up to ≈ 400 °C using TG/DTA. This synthesis method could be expanded to synthesize other transition-metal tetraborides with the following advantages:

1. Synthesis and densification can be performed in a single step in a short time and as a result less energy consumption.
2. Accurate temperature control, which is not possible in the arc melting method.
3. Improved flexibility in sample size, addressing a key limitation in the HPHT method.

Data availability

The data that support the findings of this study are available from the

corresponding author upon request.

CRediT authorship contribution statement

S.B. Dhuban: Writing – original draft, Investigation. **Hyoung-Won Son:** Writing – review & editing, Supervision, Investigation. **Takao Mori:** Writing – review & editing, Resources, Project administration, Funding acquisition, Conceptualization.

Declaration of competing interest

The authors declare that they have no known competing financial interests or personal relationships that could have appeared to influence the work reported in this paper.

Acknowledgements

Support from JST Mirai Program (JPMJMI19A1) is acknowledged. Center support from JSPS WPI Academy is also thanked.

References

[1] T. Mori, Handbook on the Physics and Chemistry of Rare-earths, 1st ed., Elsevier, North-Holland, Amsterdam, 2008.
[2] T. Mori, H. Borrmann, S. Okada, K. Kudou, A. Leithe-Jasper, U. Burkhardt, Y. Grin, Crystal structure, chemical bonding, electrical transport, and magnetic behavior of TmAl B4, Phys. Rev. B Condens Matter. Mater Phys. 76 (2007), https://doi.org/10.1103/PhysRevB.76.064404.
[3] G. Akopov, M.T. Yeung, R.B. Kaner, Rediscovering the crystal chemistry of borides, Adv. Mater. 29 (2017), https://doi.org/10.1002/adma.201604506.
[4] T. Mori, Thermoelectric and magnetic properties of rare earth borides: boron cluster and layered compounds, J. Solid State Chem. 275 (2019) 70–82, https://doi.org/10.1016/j.jssc.2019.03.046.
[5] J. Nagamatsu, N. Nakagawa, T. Muranaka, Y. Zenitani, J. Akimitsu, Superconductivity at 39 K in magnesium diboride, Nature 410 (2001) 63–64, https://doi.org/10.1038/35065039.
[6] H.Y. Chung, M.B. Weinberger, J.B. Levine, A. Kavner, J.M. Yang, S.H. Tolbert, R. B. Kaner, Synthesis of ultra-incompressible superhard rhenium diboride at ambient pressure, Science 316 (2007) (1979) 436–439, https://doi.org/10.1126/science.1139322.
[7] R. Mohammadi, A.T. Lech, M. Xie, B.E. Weaver, M.T. Yeung, S.H. Tolbert, R. B. Kaner, Tungsten tetraboride, an inexpensive superhard material, Proc. Natl. Acad. Sci. 27 (2011) 10958–10962, https://doi.org/10.1073/pnas.1102636108.
[8] E. Bykova, S.V. Ovsyannikov, M. Bykov, Y. Yin, T. Fedotenko, H. Holz, S. Gabel, B. Merle, S. Chariton, V.B. Prakapenka, N. Dubrovinskaia, A.F. Goncharov, L. Dubrovinsky, Synthesis, crystal structure, and properties of stoichiometric hard tungsten tetraboride, WB 4, J. Mater. Chem. A 37 (2022) 20111–20120, https://doi.org/10.1039/D2TA02268K.
[9] W.G. Fahrenholtz, G.E. Hilmas, Ultra-high temperature ceramics: materials for extreme environments, Scr. Mater. (2017) 94–99, https://doi.org/10.1016/j.scriptamat.2016.10.018.
[10] H. Gou, N. Dubrovinskaia, E. Bykova, A.A. Tsirlin, D. Kasinathan, W. Schnelle, A. Richter, M. Merlini, M. Hanfland, A.M. Abakumov, D. Batuk, G. Van Tendeloo, Y. Nakajima, A.N. Kolmogorov, L. Dubrovinsky, Discovery of a superhard iron tetraboride superconductor, Phys. Rev. Lett. 111 (2013), https://doi.org/10.1103/PhysRevLett.111.157002.
[11] S. Li, Q. Zheng, Y. Lv, X. Liu, X. Wang, P.Y. Huang, D.G. Cahill, B. Lv, High thermal conductivity in cubic boron arsenide crystals, Science 361 (2018) (1979) 579–581, https://doi.org/10.1126/science.aat8982.
[12] T. Mori, T. Nishimura, K. Yamaura, E. Takayama-Muromachi, High temperature thermoelectric properties of a homologous series of n-type boron icosahedra compounds: a possible counterpart to p-type boron carbide, J. Appl. Phys. 101 (2007), https://doi.org/10.1063/1.2730571.
[13] A. Sussardi, T. Tanaka, A.U. Khan, L. Schlapbach, T. Mori, Enhanced thermoelectric properties of samarium boride, J. Materiom. 1 (2015) 196–204, https://doi.org/10.1016/j.jmat.2015.07.007.
[14] H.-W. Son, D. Berthebaud, K. Yubuta, A. Yoshikawa, T. Shishido, K. Suzuta, T. Mori, New synthesis route for complex borides; rapid synthesis of thermoelectric yttrium aluminoboride via liquid-phase assisted reactive spark plasma sintering, Sci. Rep. 10 (2020) 8914, https://doi.org/10.1038/s41598-020-65818-z.
[15] L. Zhang, Y. Wang, J. Lv, Y. Ma, Materials discovery at high pressures, Nat. Rev. Mater. 2 (2017), https://doi.org/10.1038/natrevmats.2017.5.
[16] G. Akopov, I. Roh, Z.C. Sobell, M.T. Yeung, L. Pangilinan, C.L. Turner, R.B. Kaner, Effects of variable boron concentration on the properties of Superhard Tungsten Tetraboride, J. Am. Chem. Soc. 139 (2017) 17120–17127, https://doi.org/10.1021/jacs.7b08706.
[17] W. Wang, F. Peng, H. Liang, S. Guan, W. Liang, L. Zhang, M. Huang, Y. Tang, D. He, Synthesis and sintering of tungsten tetraboride and tantalum-bearing tungsten tetraboride under ultra high temperature and high pressure, Int. J. Refract. Metals. Hard. Mater. 102 (2022) 105701, https://doi.org/10.1016/j.ijrmhm.2021.105701.
[18] H. Gou, N. Dubrovinskaia, E. Bykova, A.A. Tsirlin, D. Kasinathan, W. Schnelle, A. Richter, M. Merlini, M. Hanfland, A.M. Abakumov, D. Batuk, G. Van Tendeloo, Y. Nakajima, A.N. Kolmogorov, L. Dubrovinsky, Discovery of a superhard iron tetraboride superconductor, Phys. Rev. Lett. 111 (2013) 157002, https://doi.org/10.1103/PhysRevLett.111.157002.
[19] S. Wang, X. Yu, J. Zhang, Y. Zhang, L. Wang, K. Leinenweber, H. Xu, D. Popov, C. Park, W. Yang, D. He, Y. Zhao, Crystal structures, elastic properties, and hardness of high-pressure synthesized CrB2 and CrB4, J. Superhard Mater. 36 (2014) 279–287, https://doi.org/10.3103/S1063457614040066.
[20] A.S. Mukasyan, A.S. Rogachev, D.O. Moskovskikh, Z.S. Yermekova, Reactive spark plasma sintering of exothermic systems: a critical review, Ceram. Int. 48 (2022) 2988–2998, https://doi.org/10.1016/j.ceramint.2021.10.207.
[21] R. Licheri, C. Musa, R. Orrù, G. Cao, Influence of the heating rate on the in situ synthesis and consolidation of ZrB2 by reactive spark plasma sintering, J. Eur. Ceram. Soc. 35 (2015) 1129–1137, https://doi.org/10.1016/j.jeurceramsoc.2014.10.039.
[22] C. Musa, R. Orrù, R. Licheri, G. Cao, Spark plasma synthesis and densification of TaB2 by pulsed electric current sintering, Mater. Lett. 65 (2011) 3080–3082, https://doi.org/10.1016/j.matlet.2011.06.094.
[23] N.S. Karthiselva, B.S. Murty, S.R. Bakshi, Low temperature synthesis of dense and ultrafine grained zirconium diboride compacts by reactive spark plasma sintering, Scr. Mater. 110 (2016) 78–81, https://doi.org/10.1016/j.scriptamat.2015.08.005.
[24] X. Zhang, G.E. Hilmas, W.G. Fahrenholtz, Synthesis, densification, and mechanical properties of TaB2, Mater. Lett. 62 (2008) 4251–4253, https://doi.org/10.1016/j.matlet.2008.06.052.
[25] P. Zhao, J. Zhu, H. Wang, X. Zhao, M. Li, W. Liu, B. Fan, G. Shao, H. Lu, H. Xu, R. Zhang, S.H. Lee, Dense HfB2 ceramics fabricated by high-energy ball milling and spark plasma sintering, Mater. Chem. Phys. 258 (2021), https://doi.org/10.1016/j.matchemphys.2020.123845.
[26] N.S. Karthiselva, B.S. Murty, S.R. Bakshi, Low temperature synthesis of dense TiB2 compacts by reaction spark plasma sintering, Int. J. Refract. Metals Hard. Mater. 48 (2015) 201–210, https://doi.org/10.1016/j.ijrmhm.2014.09.015.
[27] S. Ran, L. Zhang, O. Van der Biest, J. Vleugels, Pulsed electric current, in situ synthesis and sintering of textured TiB2 ceramics, J. Eur. Ceram. Soc. 30 (2010) 1043–1047, https://doi.org/10.1016/j.jeurceramsoc.2009.09.030.
[28] J. Che, Y. Long, X. Zheng, H.T. Lin, K. Plucknett, Mechanical alloying assisted spark plasma sintering of Tungsten diboride ceramics, Mater. Chem. Phys. 237 (2019), https://doi.org/10.1016/j.matchemphys.2019.121848.
[29] D. Sciti, S. Guicciardi, M. Nygren, Densification and mechanical behavior of HfC and HfB2 fabricated by spark plasma sintering, J. Am. Ceram. Soc. 91 (2008) 1433–1440, https://doi.org/10.1111/j.1551-2916.2007.02248.x.
[30] K. Sairam, J.K. Sonber, T.S.R.C. Murthy, C. Subramanian, R.K. Fotedar, R.C. Hubli, Reaction spark plasma sintering of niobium diboride, Int. J. Refract. Metals Hard. Mater. 43 (2014) 259–262, https://doi.org/10.1016/j.ijrmhm.2013.12.011.
[31] M. Qin, J. Gild, H. Wang, T. Harrington, K.S. Vecchio, J. Luo, J. Luo, Dissolving and stabilizing soft WB2 and MoB2 phases into high-entropy borides via boron-metals reactive sintering to attain higher hardness, J. Eur. Ceram. Soc. 12 (2020) 4348–4353, https://doi.org/10.1016/j.jeurceramsoc.2020.03.063.
[32] G. Tallarita, R. Licheri, S. Garroni, S. Barbarossa, R. Orrù, G. Cao, High-entropy transition metal diborides by reactive and non-reactive spark plasma sintering: a comparative investigation, J. Eur. Ceram. Soc. 40 (2020) 942–952, https://doi.org/10.1016/j.jeurceramsoc.2019.10.031.
[33] A. Knappschneider, C. Litterscheid, J. Brgoch, N.C. George, S. Henke, A. K. Cheetham, J.G. Hu, R. Seshadri, B. Albert, Manganese tetraboride, MnB4: high-temperature crystal structure, p-n transition, 55Mn NMR spectroscopy, solid solutions, and mechanical properties, Chem. Eur. J. 21 (2015) 8177–8181, https://doi.org/10.1002/chem.201406631.
[34] S. Andersson, J.-O. Carlsson, The crystal structure of MnB4, Acta. Chem. Scand. 24 (1970) 1791–1799.
[35] H. Gou, A.A. Tsirlin, E. Bykova, A.M. Abakumov, G. Van Tendeloo, A. Richter, S. V. Ovsyannikov, A.V. Kurnosov, D.M. Trots, Z. Konôpková, H.P. Liermann, L. Dubrovinsky, N. Dubrovinskaia, Peierls distortion, magnetism, and high hardness of manganese tetraboride, Phys Rev B Condens Matter Mater Phys 89 (2014), https://doi.org/10.1103/PhysRevB.89.064108.
[36] A. Knappschneider, C. Litterscheid, N.C. George, J. Brgoch, N. Wagner, J. Beck, J. A. Kurzman, R. Seshadri, B. Albert, Peierls-distorted monoclinic MnB4 with a mn-Mn bond, Angewandte Chemie - Int. Edition 53 (2014) 1684–1688, https://doi.org/10.1002/anie.201306548.
[37] H. Gou, Z. Li, H. Niu, F. Gao, J. Zhang, R.C. Ewing, J. Lian, Unusual rigidity and ideal strength of CrB 4 and MnB 4, Appl. Phys. Lett. 100 (2012), https://doi.org/10.1063/1.3692777.
[38] B. Wang, X. Li, Y.X. Wang, Y.F. Tu, Phase stability and physical properties of manganese borides: a first-principles study, J. Phys. Chem. C 115 (2011) 21429–21435, https://doi.org/10.1021/jp2073683.
[39] S. Ma, K. Bao, Q. Tao, Y. Huang, C. Xu, L. Li, X. Feng, X. Zhao, P. Zhu, T. Cui, Investigation the origin and mechanical properties of unusual rigid diamond-like net analogues in manganese tetraboride, Int. J. Refract. Metals. Hard. Mater. 85 (2019), https://doi.org/10.1016/j.ijrmhm.2018.12.010.
[40] F.-Z. Dai, Y. Zhou, A modified theoretical model of intrinsic hardness of crystalline solids, Sci. Rep. 6 (2016) 33085, https://doi.org/10.1038/srep33085.
[41] V. Homolová, J. Kepič, A. Zemanová, O. Zobač, Experimental study of phase composition of B-Fe-Mn-V alloys and thermodynamic calculations of phase equilibria in the B-Mn-V and B-Fe-Mn-V systems, Adv. Mater. Sci. Eng. 2018 (2018), https://doi.org/10.1155/2018/3950980.

[42] G.J. Fan, F.Q. Guo, Z.Q. Hu, M.X. Quan, K. Lu, Amorphization of selenium induced by high-energy ball milling, Phys. Rev. B 55 (1997) 11010–11013, https://doi.org/10.1103/PhysRevB.55.11010.
[43] H. Bakker, G.F. Zhou, H. Yang, Mechanically driven disorder and phase transformations in alloys, Prog. Mater Sci. 39 (1995) 159–241, https://doi.org/10.1016/0079-6425(95)00001-1.
[44] A.S. Mukasyan, A.S. Rogachev, D.O. Moskovskikh, Z.S. Yermekova, Reactive spark plasma sintering of exothermic systems: a critical review, Ceram. Int. 48 (2022) 2988–2998, https://doi.org/10.1016/j.ceramint.2021.10.207.
[45] H. Niu, X.-Q. Chen, W. Ren, Q. Zhu, A.R. Oganov, D. Li, Y. Li, Variable-composition structural optimization and experimental verification of MnB_3 and MnB_4, Phys. Chem. Chem. Phys. 16 (2014) 15866–15873, https://doi.org/10.1039/C4CP01339E.
[46] G. Tallarita, R. Licheri, S. Garroni, S. Barbarossa, R. Orrù, G. Cao, High-entropy transition metal diborides by reactive and non-reactive spark plasma sintering: a comparative investigation, J. Eur. Ceram. Soc. 40 (2020) 942–952, https://doi.org/10.1016/j.jeurceramsoc.2019.10.031.
[47] R. Mohammadi, C.L. Turner, M. Xie, M.T. Yeung, A.T. Lech, S.H. Tolbert, R. B. Kaner, Enhancing the hardness of superhard transition-metal borides: molybdenum-doped tungsten tetraboride, Chem. Mater. 28 (2016) 632–637, https://doi.org/10.1021/acs.chemmater.5b04410.